ADVANCES IN ATMOSPHERIC SCIENCES, VOL. 30, NO. 1, 2013, 67–76

# The Propagation of Wave Packets and Its Relationship with the Subtropical Jet over Southern China in January 2008

ZUO Qunjie[1,2,3] (左群杰), GAO Shouting*[1,4] (高守亭), and LÜ Daren[3] (吕达仁)

[1] *Laboratory of Cloud-Precipitation Physics and Severe Storms, Institute of Atmospheric Physics, Chinese Academy of Sciences, Beijing* 100029

[2] *University of Chinese Academy of Sciences, Beijing* 100049

[3] *Key Laboratory of Middle Atmosphere and Global Environment Observation, Institute of Atmospheric Physics, Chinese Academy of Sciences, Beijing* 100029

[4] *State Key Laboratory of Severe Weather, Chinese Academy of Meteorological Sciences, Beijing* 100029

(Received 12 October 2011; revised 13 February 2012)

**ABSTRACT**

The propagation of wave packets and its relationship with the subtropical jet was investigated for the period 26–29 January 2008 over southern China using ECMWF Interim re-analysis data. Wave packets propagated from the north to the south side of an upper front with eastward development along the upper front during this period. Due to the eastward development of propagation, the acceleration of geostrophic westerly winds shifted eastward along the front. There were two primary sources of the propagation of wave packets at around 30°N. The first was the temperature inversion layer below 500 hPa, and the second was baroclinic zones located along the polarward flank of the subtropical jet in the middle and upper troposphere. Most wave packets propagated horizontally from the baroclinic zones and then converged on the zero meridional gradients of zonal winds.

**Key words**: propagation of wave packets, wave-mean flow interaction, subtropical jet, geopotential anomalies, snowstorms

**Citation**: Zuo, Q. J., S. T. Gao, and D. R. Lü, 2013: The propagation of wave packets and its relationship with the subtropical jet over southern China in January 2008. *Adv. Atmos. Sci.*, **30**(1), 67–76, doi: 10.1007/s00376-012-1197-6.

## 1. Introduction

In winter, the climate over China is characterized by low temperatures, snowstorms, and freezing rain resulting from the influence of a cold surge that is one of the most prominent features of the Asian winter monsoon (Ding and Krishnamurti, 1987; Dong et al., 1994; Wu and Chan, 1995; Zhang et al., 1996; Wu and Chan, 1997; Zhang et al., 1999; Zhang and Sumi, 2002; Huang et al., 2007).

In January and early February 2008, an unprecedented storm affected China, leading to extreme and long-lasting low temperatures, blizzard conditions and freezing rain over southern China. According to statistics released by the Ministry of Civil Affairs of China, the direct socioeconomic loss was estimated to be more than $22.3 billion, and indirect losses even greater (Peng and Peng, 2008; Zhao et al., 2008).

There were two critical airflows involved in this extreme event: cold air, which affected southern China because of the persistence of a blocking pattern over the northern Asian continent in the middle latitudes; and a warm and moist flow of air provided by a strong trough that existed over the Bay of Bengal. Several physical processes are thought to have played crucial roles in intensifying these two special flows:

(1) The maintenance of the western Pacific subtropical high may have promoted the transport of

*Corresponding author: GAO Shouting, gst@mail.iap.ac.cn

warm-moist air into southeast China.

(2) The variation (southeastward shift and intensification) of the Middle East jet stream and the positive phase of the Arctic Oscillation could have favored intrusions of cold air into East Asia, enhancing water vapor transport from western Asia and the Bay of Bengal to China (Wen et al., 2009).

(3) An anomalous subtropical western Pacific high over the East Asian coast may have decelerated the eastward propagation of weather systems to the Pacific and enhanced water vapor transport from the northern South China Sea to the snowstorm regions (Wen et al., 2009).

(4) When the cold air encountered the warm air over southern China along a quasi-stationary front, the water moisture would have condensed and became snow or freezing rain (Wen et al., 2009; Zhou et al., 2009; Shi et al., 2010).

(5) A deep inversion layer in the lower troposphere may also have been important, in terms of its association with the extended snow cover over most of central and southern China (Zhou et al., 2009).

Among the factors mentioned above, the Siberia blocking may have been the most important because it would have established and maintained the cold conditions over southern China (Zhou et al., 2009). Furthermore, another significant and distinct synoptic characteristic of this severe freezing rain and snowstorm event was an east–west or northeast–southwest orientation and rare (hardly ever observed over China during winters prior to 2008) quasi-stationary front located over southern China (Sun and Zhao, 2010). There were different precipitation types occurring during the period 25–30 January 2008 in the western and eastern parts of the quasi-stationary front (Sun and Zhao, 2010), detailed observational and theoretical studies of which can be found in Sun and Zhao (2010).

The role of tropospheric jet streaks in the development of severe convective systems has been summarized by, for example, Pettersen (1956) and Newton (1963, 1967). Their primary role is to transport cool and dry air that enhances upper level divergence and transports sensible heat downstream from the convection region. The interaction between upper and lower tropospheric jets can create a region of convective instability within which severe weather ultimately occurs (Uccellini and Johnson, 1979). Furthermore, the interaction of transverse vertical circulations associated with two separate upper level jet streaks can also produce severe weather (Uccellini and Kocin, 1987).

In most diagnostic studies, the conventional Eliassen-Palm (E-P) flux has proven to be a powerful tool for diagnosing the interaction between wave packets and zonal-mean flow on the meridional plane (Andrews and Mcintyre, 1976; Edmon et al., 1980; McIntyre, 1982; Andrews et al., 1987). However, it cannot represent the propagation in the zonal direction. The extended E-P flux, as formulated by Hoskins et al. (1983) and Trenberth (1986), has been widely used, since it can represent the zonal propagation of small-amplitude wave packets. Plumb (1985) derived a wave-activity flux to represent 3-D wave propagation. Based on Plumb's work, Takaya and Nakamura (2001) derived a new 3-D wave-activity flux containing the group velocity.

In this paper, we report upon work in which the planetary wave activity flux introduced by Plumb (1985) was adopted to study the interaction between wave packets and the subtropical jet during the extreme event of January/February 2008 over southern China. Following this introduction, the data and analysis are described in section 2. Some details about the daily mean subtropical jet over southern China from 26 to 29 January 2008 are given in section 3. The propagation of wave packets and its relationship with the subtropical jet are presented in section 4. And finally, a short discussion is presented in section 5.

## 2. Data and analysis

The study was based on six-hourly ECMWF (European Centre for Medium-Range Weather Forecasts) Interim Re-analysis (ERA-Interim, Simmons et al., 2007) data for the year 2008. The ERA-Interim data have a horizontal $1.5^\circ \times 1.5^\circ$ resolution on 37 pressure levels from 1000 to 1 hPa, with 60 vertical hybrid levels for the spectral model. A 4-D Variational (4D Var.) data assimilation system with 12-hour cycling is used with output every six hours. A new humidity analysis has recently been added into the assimilation, and variational bias correction of satellite radiance data and other improvements were made before assimilation took place.

The snowstorm, which was a once-in-50-years event (or once in 100 years for some regions) (Shi et al., 2010) was organized into four stages from January to February 2008: 10–16 January (stage I); 18–22 January (stage II); 25–30 January (stage III); and 31 January to 2 February (stage IV). The most severe and persistent freezing rain occurred between 25° and 30°N, in the areas of Hunan, Guizhou, and Jiangxi Provinces (Sun and Zhao, 2010). Only the data recorded during the period 26–29 January (stage III) were selected for the study because the most severe freezing rain and snowstorm took place during this stage.

The wave activity flux $\boldsymbol{F}_{\rm s}$, introduced by Plumb (1985), was calculated to depict a propagating packet

of planetary waves in 3-D space. It is quite useful to analyze the source region from which planetary waves propagate in 3-D space, and the definition of $\boldsymbol{F}_{\rm s}$ on a sphere is derived in log-pressure coordinates as follows:

$$\boldsymbol{F}_{\rm s}=p\cos\varphi\begin{pmatrix} v'^2-\dfrac{1}{2\Omega a\sin 2\varphi}\dfrac{\partial(v'\Phi')}{\partial\lambda} \\ -u'v'+\dfrac{1}{2\Omega a\sin 2\varphi}\dfrac{\partial(u'\Phi')}{\partial\lambda} \\ \dfrac{2\Omega\sin\varphi}{S}\left[v'T'-\dfrac{1}{2\Omega a\sin 2\varphi}\dfrac{\partial(T'\Phi')}{\partial\lambda}\right]\end{pmatrix}. \tag{1}$$

Here, $p$ is a ratio between pressure (hPa) and 1000 hPa, $(u, v)$ represents zonal and meridional geostrophic winds, $\Phi$ is geopotential, and $T$ is temperature. The prime denotes small perturbations to a steady zonal flow. $\Omega$ is the Earth's rotation rate, $a$ is the Earth's radius, and $(\varphi, \lambda)$ is the latitude and longitude. $S$ is the static stability, which is defined as

$$S=(\partial\widehat{T}/\partial z)+\kappa\widehat{T}/H\ . \tag{2}$$

$\widehat{T}$ is global areal average temperature, and $H$ is the constant-scale height.

## 3. Jet stream over southern China

The daily mean local geostrophic westerly winds (referred to simply as westerly winds hereafter) at 300 hPa from 26–29 January 2008 are shown in Fig. 1. In the mid- and upper-troposphere, the subtropical jet was located around 25°N and there were obvious accelerations of local subtropical jet over China. A local westerly winds maximum over the south of the Tibetan Plateau at around (25°N, 90°E) was in excess of 70 m s$^{-1}$, and local westerly winds travelling at about 50–60 m s$^{-1}$ were located over Guizhou Province on 26 January (Fig. 1a). On 27 January, the speed of local westerly winds maximum over the south of the

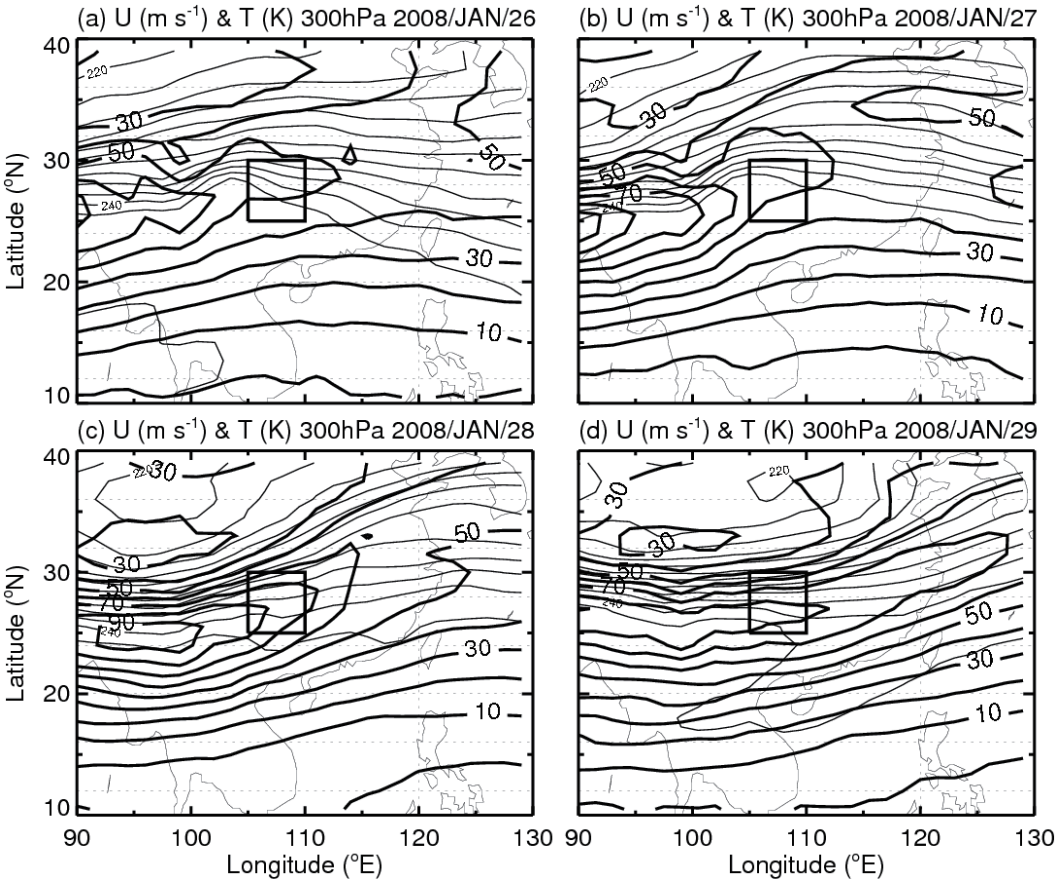


**Fig. 1.** The daily mean distributions of geostrophic zonal wind (thick solid lines) and temperature (thin solid lines) at 300 hPa over southern China on (a)–(d) 26–29 Jan 2008. Guizhou Province is labeled by the bold-black square (25°–30°N, 105°–110°E). The contour intervals are 10 m s$^{-1}$ for the zonal wind and 2 K for the temperature.

Tibetan Plateau increased from about 70 m $s^{-1}$ to more than 90 m $s^{-1}$ compared to 26 January, whilst over Guizhou Province they remained at 50–60 m $s^{-1}$ (Fig. 1b). From 27–28 January, the local westerly winds maximum shifted eastward and finally located at around (25°N, 95°E) on 28 January; and thus, over Guizhou Province, these winds increased from 50–60 m $s^{-1}$ to 70–80 m $s^{-1}$ (Figs. 1b and c). From 28–29 January, the local westerly winds maximum over the southeast of the Tibetan Plateau at around (25°N, 95°E) decreased down to about 80 m $s^{-1}$, but over Guizhou Province the local westerly winds increased to more than 80 m $s^{-1}$ (Figs. 1c and d). Over the east of Guizhou Province, an increase in local westerly wind speed also occurred, but less intensely than over the west of the province, and the province as a whole. For instance, at 114°E, local westerly winds increased from less than 50 m $s^{-1}$ on 26 and 27 January (Figs. 1a and b) to about 60 m $s^{-1}$ on 28 January (Fig. 1c), and then to 70–80 m $s^{-1}$ on 29 January (Fig. 1d).

An upper troposphere quasi-stationary front can be seen to have occurred over the south of the Tibetan Plateau at around 30°N in Fig. 1a. The variation of this front with time is related to the acceleration of local westerly winds, and the maximum of local westerly winds in this case was located on the warm side of the front. From 26 to 28 January (Figs. 1a–c) the front extended eastward and strengthened as the local westerly winds maximum shifted eastward and increased. From 28–29 January (Figs. 1c and d), the front extended continually eastward but weakened as the local westerly winds maximum shifted continually eastward but decreased.

The occurrence of this upper quasi-stationary front over southern China is linked to the simultaneous occurrence of a quasi-stationary front in the lower troposphere, which, when either east–west- or northeast–southwest-oriented, is itself formed during severe precipitation stages over southern China, and sometimes along the Yangtze River basin. However, such quasi-stationary fronts rarely appear during winters in southern China (Sun and Zhao, 2010).

## 4. Wave propagation and wave-flow interaction in the jet

As described in section 3, the local westerly winds over southern China accelerated, and there was an eastward development of this acceleration. But how, within this acceleration process, did the geopotential change in the westerly jet? To address this question, we first focus on the development of geopotential anomalies over South China. These anomalies were calculated by subtracting the 23-yr January average of daily values from the zonal-mean geopotential data recorded during 26–29 January 2008.

The development of geopotential anomalies at 500 hPa, 300 hPa and 200 hPa, which were averaged between 24°N and 30°N, are shown in Fig. 2. The eastward progression of negative geopotential anomalies

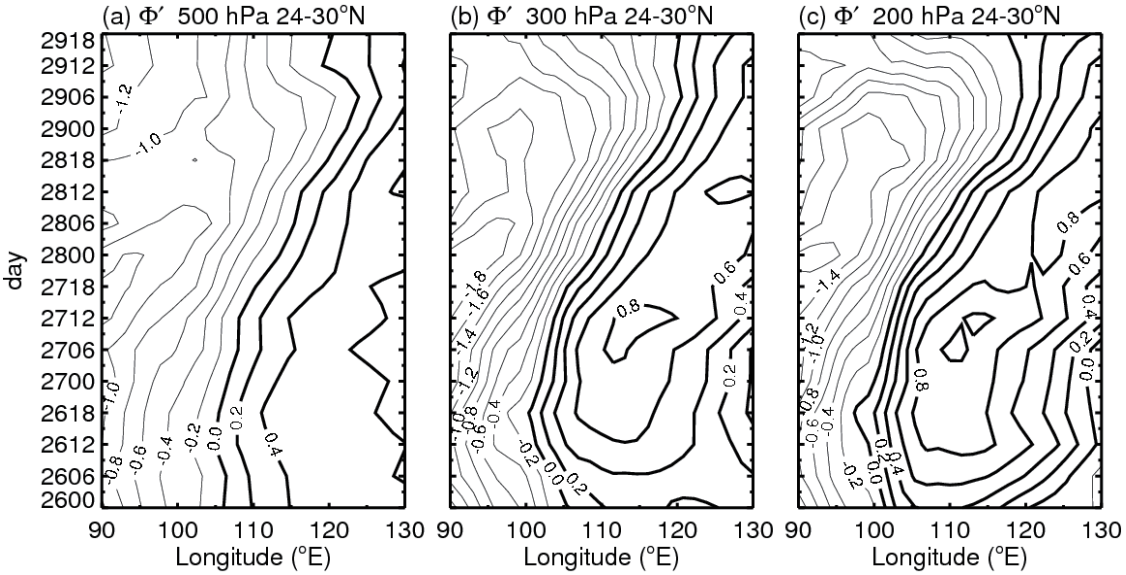


**Fig. 2.** Temporal evolutions of geopotential ($\Phi$) anomalies averaged between 24°N and 30°N from 0000 UTC 26 to 1800 UTC 29 Jan 2008 at 500 hPa (a), 300 hPa (b) and 200 hPa (c). The anomalies are the deviation from the zonal climatology of January, 1989–2011. The solid thin and thick lines denote the negative and positive values, respectively. The contour interval is $0.2\times10^3$ $m^2$ $s^{-2}$.

at these three pressure levels can be clearly seen for the period 27–29 Jan 2008. Moreover, these progressions were different at different times during these three days. From 0000 UTC 26 to 0000 UTC 27, the anomalies were almost stable in the latitude belt. Then, from 0000 UTC 27 to 0000 UTC 28, rapid eastward propagation of the anomalies took place at the three pressure levels between 90° to 100°E. Following the geostrophic wind relationship, there was a local development of westerly winds, which can be seen in Figs. 1a and b. From 0000 UTC 28 to 0000 UTC 29, the center of the anomalies appeared at around 100°E, and the anomalies continued to migrate eastward. Because of the development of these anomalies, the westerly winds strengthened at around 100°E and the jet streak moved eastward (Figs. 1b and c). From 0000 UTC 29 to 1800 UTC 29, the anomalies propagated to around 120°E, with an increase of the westerly winds in the same area.

Previously, Sun and Zhao (2010) used infrared data for cloud-top temperatures from the Chinese Fengyun (FY-2C) satellite to analyze the activities of mesoscale systems propagating eastward from the Tibetan Plateau toward eastern China. Their results showed that cloud clusters were limited over the Tibetan Plateau during 26–27 January 2008, and then moved eastward to affect the middle and lower reaches of the Yangtze River from 27–29 January, leading to the heavy precipitation from 27–28 January. After 29 January, their data showed that the systems over the Tibetan Plateau became weaker, but were still relatively active and moved eastward (Fig. 9a in Sun and Zhao, 2010). These results relating to the variation of cloud clusters from 26–29 January 2008 agrees reasonably well with our results on the variation of negative geopotential anomalies over southern China.

Some authors have studied the relationship of wave propagation with rainfall and indicated that quasi-stationary waves play important roles in the rainfall over South America by affecting blocking episodes in the southeast Pacific near the west coast of South America during El Niño events (Rutllant and Fuenzalida, 1991; Renwick and Revell, 1999; Marques and Rao, 1999, 2000; Rao et al., 2000, 2002). In the context of our results, a quasi-stationary blocking high over Siberia led to advection of dry and cold Siberian air down to central and southern China. This persistent system remained in place for three weeks and might have been due to strong nonlinear interactions among waves and mean flow (Zhou et al., 2009). However, quasi-stationary waves not only affected the blocking, but also the subtropical jet. Accordingly, the wave activity flux introduced by Plumb (1985) was calculated to study the propagation of waves in 3-D space in order to provide a deeper understanding of the eastward progression of geopotential anomalies and the jet. The longitude–latitude cross sections (10°–40°N, 90°–130°E) of daily temperature and horizontal components of daily wave activity flux from Eq. (1) at 300 hPa are plotted in Fig. 3.

On 26 January (Fig. 3a), wave packets propagated southeastward from the cold area over the south of the Tibetan Plateau at around (30°N, 95°E) and converged over the west of Guizhou Province. By 27 January (Fig. 3b), the propagation of wave packets became stronger compared to 26 January, the source region was still the cold area over the south of the Tibetan Plateau, and wave packets still converged over the west of Guizhou Province. This strengthening of the propagation of wave packets only appeared over the west of Guizhou Province from 26–27 January, and was consistent with the decrease of the negative geopotential anomalies during the same period over the same area shown in Fig. 2b. This process was also consistent with the acceleration of local westerly winds over the west of Guizhou Province shown in Figs. 1a and b. From 27–28 January (Figs. 3b and c), the propagation of wave packets strengthened continually over the west of Guizhou Province and had remarkably appeared over the northeast of Guizhou Province. The increase and northeastward development of the propagation during this period was associated with the decrease and eastward development of the negative geopotential anomalies shown in Fig. 2b. This process was also associated with the acceleration of local westerly winds in the corresponding area shown in Figs. 1b and c. From 28–29 January (Figs. 3c and d), the propagation of wave packets weakened over the west of Guizhou Province, but strengthened over the east of Guizhou Province. The development of the propagation of wave packets during this period was related with the increase of the negative geopotential anomalies over the west of Guizhou Province and the decrease from positive to negative geopotential anomalies over the east of Guizhou Province shown in Fig. 2b. This process was also related to the deceleration of local westerly winds over the west of Guizhou Province and their acceleration over the east of Guizhou Province shown in Figs. 1c and d. Note, the behavior of the propagation of the wave packets was also consistent with the behavior of cloud clusters, mentioned above.

Clear evidence was observed for the propagation of wave packets, the variation of westerly winds, and the development of geopotential anomalies. The eastward propagation of wave packets developed along the upper front (Figs. 3a and b) and reached a trough over the west of Guizhou Province, strengthening it (Fig. 2b). The development of this trough tended to accelerate

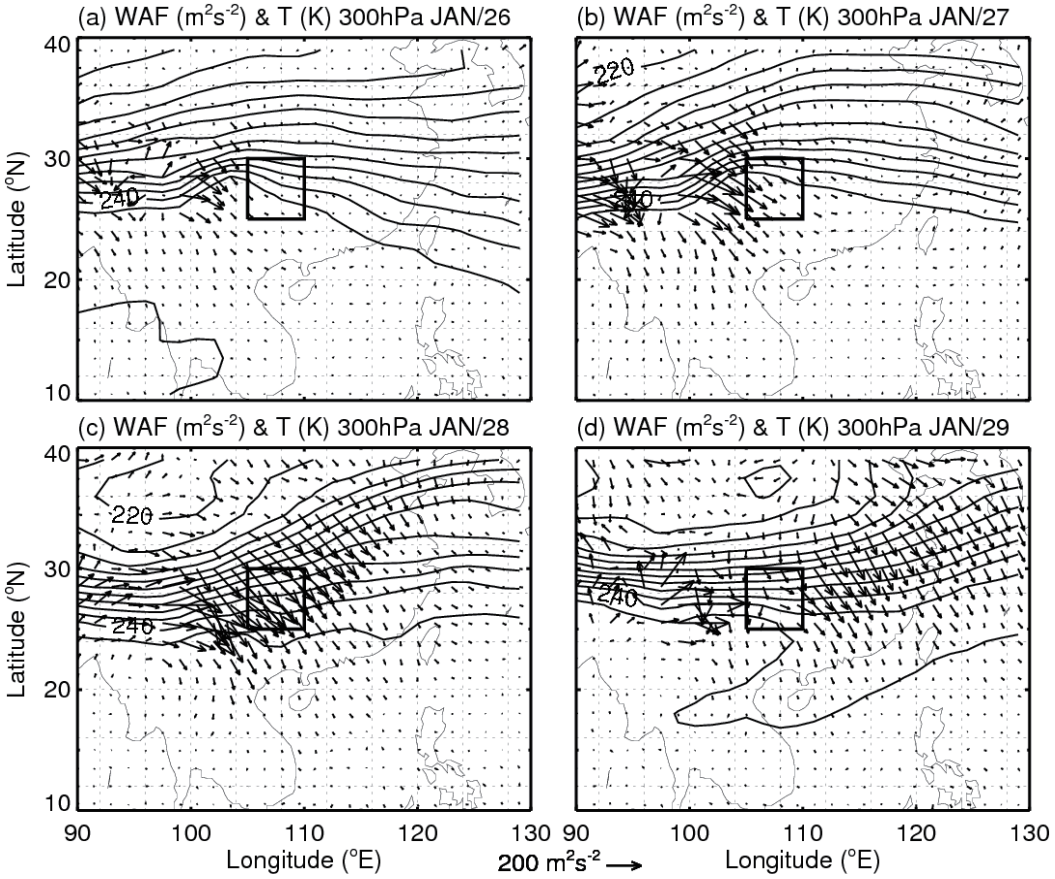


**Fig. 3.** Horizontal propagation of wave packets at 300 hPa on (a)–(d) 26–29 Jan 2008. The temperature contour interval is 2 K. Vectors show Plumb's wave activity flux in units of $m^2\ s^{-2}$. Scales of vectors are shown in the middle lower region of the panels. Guizhou Province is labeled by a bold-black square (25°–30°N,105°–110°E).

the westerly winds and increase the vertical velocity over the exit of the jet. Because of the vigorous convection, a low cloud-top temperature appeared over the west of Guizhou Province. When the development of the propagation of wave packets was eastward (Figs. 3b and c), the trough developed eastward (Fig. 2b). Consequently, the westerly winds accelerated (Figs. 1b and c) and the cloud-top temperature decreased over the east of Guizhou Province. These factors provided favorable environmental conditions for the appearance of the extreme weather event over southern China.

Insight into the relationships between the propagation of wave packets and local westerly winds was gained by looking at the latitude–height cross sections of temperature, westerly winds and Plumb's wave activity flux at 106.5°E, 114°E and 120°E (Fig. 4). As Fig. 4 shows, in the lower troposphere, under 500 hPa, the westerly maximum was located at around 25°N. The westerly maximum intensified and shifted polarward with altitude so that at about 200 hPa the maximum was located at about 30°N and in excess of 80 $m\ s^{-1}$. This wind structure was associated with three regions of strong meridional temperature gradients at about 30°N. One of these was located in the lower troposphere under 500 hPa, which was an obvious temperature inversion layer. The second appeared in the middle troposphere between about 500 hPa and 250 hPa. The third was in the upper troposphere above 250 hPa. The last two strong meridional temperature gradients were opposite and can be referred to as baroclinic zones, which were located along the polarward flank of the subtropical jet (Fig. 4). These baroclinic zones corresponded to the front in the latitude–longitude plane (Fig. 3).

On 26 January at 106.5°E, there was only a small amount of propagation of wave packets upward and then equatorward from the lower troposphere temperature inversion layer under 500 hPa, converging around the zero meridional gradients of westerly winds (Fig. 4a). From 27–28 January, the propagation of

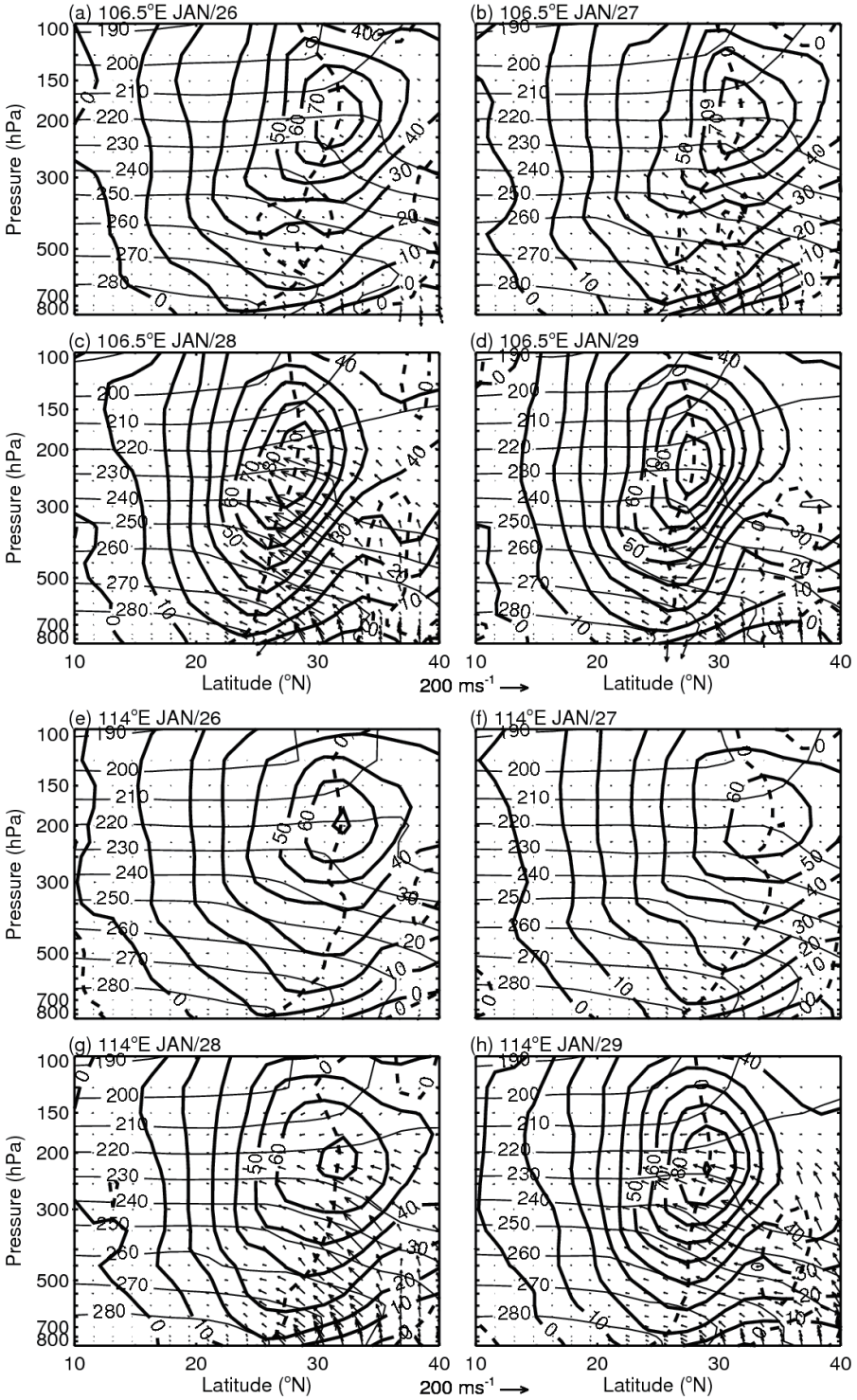


**Fig. 4.** Latitude–height cross sections of temperature (thin solid lines), zonal winds (thick solid lines), and Plumb's wave activity flux (vectors) at 106.5°E (a–d), 114°E (e–h) and 120°E (i–l). The thick dashed lines are zero meridional gradients of zonal winds. Contour intervals in temperature and zonal winds are 10 K and 10 m $s^{-2}$, respectively. Plumb's wave activity flux vectors are in units of $m^2$ $s^{-2}$. Scales of vectors are shown in the middle regions of the lower panels. The vertical component of Plumb's wave activity flux is multiplied by $10^4$. Dates are 26, 27, 28 and 29 January, respectively.

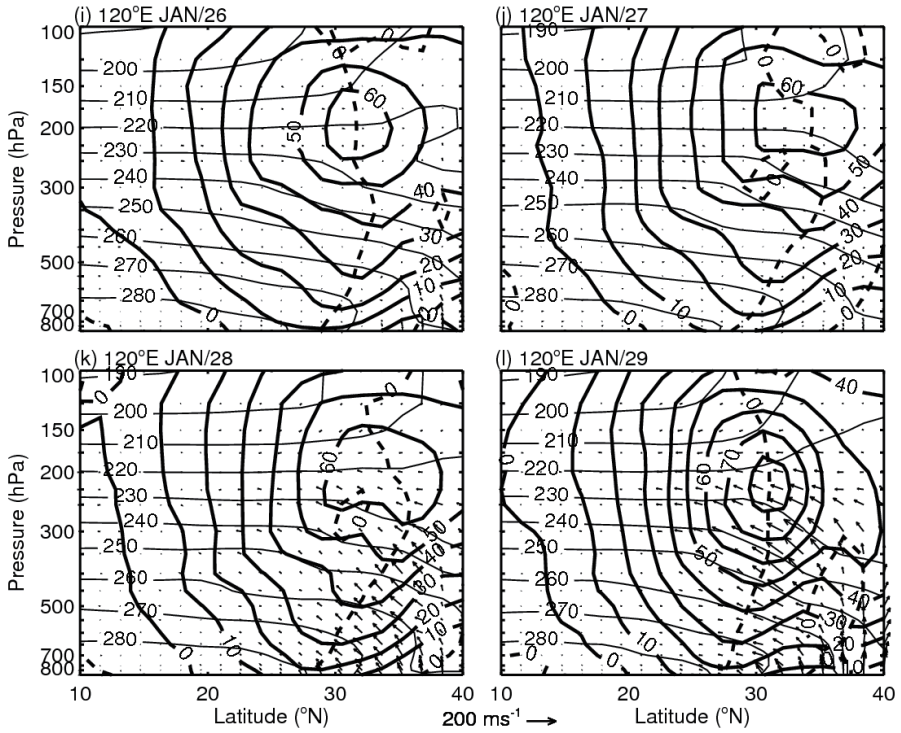


**Fig. 4.** (Continued).

wave packets gradually strengthened, and there were three obvious source regions of the propagation during this period. One was the lower troposphere temperature inversion layer. Wave packets propagated upward from this area and then equatorward, and finally converged around the zero meridional gradients of westerly winds. This behavior of wave packets only affected lower tropospheric circulation. The second was the middle troposphere baroclinic zone. From this area, most of the wave packets propagated upward, as well as equatorward, at around 30°N, and then converged around the zero meridional gradients of westerly winds. The third was the upper troposphere baroclinic zone above 250 hPa. Wave packets propagated weakly from this region, downward and equatorward. On 29 January, the propagation became weaker than that on 28 January, and the direction of it in the middle troposphere baroclinic zone was rather horizontal and equatorward at around 30°N. Over the east of Guizhou Province (Figs. 4e–l), the propagation behavior of the wave packets was the same as those over the west of Guizhou Province, but weaker in intensity.

## 5. Discussion and conclusions

The propagation of wave packets and its relationship with the acceleration of local westerly winds in the middle-upper troposphere was investigated during the period 26–29 January 2008 over southern China.

Horizontally, wave packets propagated from the north to the south side of the upper front. Propagation developed eastward along the upper front during 27–29 January, and this development corresponded to the eastward shift of acceleration of local westerly winds. The propagation of wave packets intensified the negative geopotential anomalies, and hence the meridional gradient of geopotential strengthened. Following the geostrophic wind relationship, geostrophic winds would increase in this situation. With the eastward development of the propagation of wave packets along the upper front, the geopotential anomalies and the acceleration of local westerly winds shifted eastward.

Vertically, there were two primary sources of propagation at around 30°N. The first was the temperature inversion layer below 500 hPa, from which wave packets propagated upward, as well as equatorward, and only affected the lower troposphere under 500 hPa. We do not discuss this case in any depth because the propagation of wave packets there may be affected by complicated terrain. The second source was baroclinic zones in the middle and upper troposphere, which were located along the polarward flank of the subtropical jet. Most of the wave packets propagated from the baroclinic zones horizontally and then converged on the zero meridional gradients of local westerly winds.

***Acknowledgements.*** We are grateful to the ECMWF for making their datasets readily available on-

line. This work was supported by the National Natural Science Foundation of China (Grant Nos. 40930950 and 40921160379), the Chinese Academy of Meteorological Sciences State Key Laboratory of Severe Weather (LaSW; Grant No. 2011LASW-A01) and the National Basic Research Project of China under Grant No. 2012CB417201.

## REFERENCES

Andrews, D. G., and M. E. Mcintyre, 1976: Planetary waves in horizontal and vertical shear: The generalized Eliassen-Palm relation and the mean zonal circulation. *J. Atmos. Sci.*, **33**, 2031–2048.

Andrews, D. G., J. R. Holton, and C. B. Leovy, 1987: *Middle Atmosphere Dynamics.* Academic Press, 489pp.

Ding, Y., and T. N. Krishnamurti, 1987: Heat budget of the Siberian high and the winter monsoon. *Mon. Wea. Rev.*, **115**, 2428–2449.

Dong, M., L. Chen, and H. Liao, 1994: A numerical study of the impact of sea surface temperature over the western Pacific warm pool on wintertime atmospheric circulation. *Acta Oceanologica Sinica*, **16**, 39–49. (in Chinese)

Edmon, H. J., B. J. Hoskins, and M. E. McIntyre, 1980: Eliassen-Palm cross sections for the troposphere. *J. Atmos. Sci.*, **37**, 2600–2616.

Hoskins, B. J., I. N. James, and G. H. White, 1983: The shape, propagation and mean-flow interaction of large-scale weather systems. *J. Atmos. Sci.*, **40**, 1595–1612.

Huang, R., K. Wei, J. Chen, and W. Chen, 2007: The East Asian winter monsoon anomalies in the winters of 2005 and 2006 and their relations to the quasi-stationary planetary wave activity in the Northern Hemisphere. *Chinese J. Atmos. Sci.*, **31**, 1033–1048. (in Chinese)

Marques, R. F. C., and V. B. Rao, 1999: A diagnosis of a long-lasting blocking event over the Southeast Pacific Ocean. *Mon. Wea. Rev.,* **127**, 1761–1775.

Marques, R. F. C., and V. B. Rao, 2000: Interannual variations of blockings in the Southern Hemisphere and their energetics. *J. Geophys. Res.,* **105**(D4), 4625–4636.

McIntyre, M. E., 1982: How well do we understand the dynamics of stratospheric warmings? *J. Meteor. Soc. Japan*, **60**, 37–65.

Newton, C. W., 1963: Dynamics of severe convective storms. *Meteor. Monogr.*, No. 27, Amer. Meteor. Soc., 33–35.

Newton, C. W., 1967: Severe convective storms. *Advances in Geophysics*, **12**, 257–303.

Peng, K., and H. Peng, 2008: A rare snowstorm disaster in China. *Science News,* **5**, 15–17. (in Chinese)

Pettersen, S., 1956: *Weather Analysis and Forecasting.* Vol. 2*, Weather and Weather Systems*, McGraw-Hill, 191–195.

Plumb, R. A., 1985: On the three-dimensional propagation of stationary waves. *J. Atmos. Sci.*, **42**, 217–229.

Rao, V. B., S. H. Franchito, and J. P. R. Fernandez, 2000: Comments on "Blocking over the South Pacific and Rossby wave propagation". *Mon. Wea. Rev.*, **128**, 4160–4161.

Rao, V. B., S. R. Chapa, J. P. R. Fernandez, and S. H. Franchito, 2002: A diagnosis of rainfall over South America during the 1997/98 El Niño Event. Part II: Roles of water vapor transport and stationary waves. *J. Climate*, **15**, 512–521.

Renwick, J. A., and M. J. Revell, 1999: Blocking over the South Pacific and Rossby wave propagation. *Mon. Wea. Rev.,* **127**, 2233–2247.

Rutllant, J., and H. Fuenzalida, 1991: Synoptic aspects of the central Chile rainfall variability associated with the Southern Oscillation. *International Journal of Climatology*, **11**, 63–76.

Shi, X., X. Xu, and C. Lu, 2010: The dynamic and thermodynamic structures associated with a series of heavy precipitation events over China in January 2008. *Wea. Forecasting*, **25**, 1124–1141.

Simmons, A., S. Uppala, D. Dee, and S. Kobayashi, 2007: ERA-Interim: New ECMWF reanalysis products from 1989 onwards. Newsletter 110-Winter 2006/07, ECMWF, 11pp.

Sun, J. H., and S. X. Zhao, 2010: The impacts of multiscale weather systems on freezing rain and snowstorms over southern China. *Wea. Forecasting*, **25**, 388–407.

Takaya, K., and H. Nakamura, 2001: A formulation of a phase-independent wave-activity flux for stationary and migratory quasi-geostrophic eddies on a zonally varying basic flow. *J. Atmos. Sci.*, **58**, 608–627.

Trenberth, K. E., 1986: An assessment of the impact of transient eddies on the zonal flow during a blocking episode using localized Eliassen-Palm flux diagnostics. *J. Atmos. Sci.*, **43**, 2070–2087.

Uccellini, L., and D. R. Johnson, 1979: The coupling of upper and lower tropospheric jet streaks and implications for the development of severe convective storms. *Mon. Wea. Rev.*, **107**, 682–703.

Uccellini, L. W., and P. J. Kocin, 1987: The interaction of jet streak circulations during heavy snow events along the east coast of the United States. *Wea. Forecasting*, **2**, 298–308.

Wen, M., S. Yang, A. Kumar, and P. Zhang, 2009: An analysis of the large-scale climate anomalies associated with the snowstorms affecting China in January 2008. *Mon. Wea. Rev.,* **137**, 1111–1131.

Wu, M. C., and J. C. L. Chan, 1995: Surface features of winter monsoon surges over South China. *Mon. Wea. Rev.*, **123**, 662–680.

Wu, M. C., and J. C. L. Chan, 1997: Upper-level features associated with winter monsoon surges over South China. *Mon. Wea. Rev.*, **125**, 317–340.

Zhang, R., and A. Sumi, 2002: Moisture circulation over East Asia during the El Niño episode in northern winter, spring, and autumn. *J. Meteor. Soc. Japan*, **80**, 213–227.

Zhang, R., A. Sumi, and M. Kimoto, 1996: Impact of El Niño on the East Asian monsoon: A diagnostic study of the '86/87 and '91/92 events. *J. Meteor. Soc. Japan*, **74**, 49–62.

Zhang, R., A. Sumi, and M. Kimoto, 1999: A diagnostic study of the impact of El Niño on the precipitation in China. *Adv. Atmos. Sci.*, **16**, 229–241.

Zhao, L., and Coauthors, 2008: Disasters and its impact of a severe snow storm and freezing rain over southern China in January 2008. *Climatic and Environmental Research*, **13**, 556–566. (in Chinese)

Zhou, W., J. C. L. Chan, W. Chen, J. Ling, J. G. Pinto, and Y. Shao, 2009: Synoptic-scale controls of persistent low temperature and icy weather over southern China in January 2008. *Mon. Wea. Rev.*, **137**, 3978–3991.